Photon Factory Activity Report 2001 #19B
–Users' Report–

15C/2000G038

Anomalous oscillation of an X-ray equal-inclination fringe pattern observed in ultra plane-wave topographs

Jun-ichi YOSHIMURA*[1], Keiichi HIRANO[2]
[1]Faculty of Engineering, Yamanashi University, 4-3-11 Takeda, Kofu, Yamanashi 400-8511, Japan
[2]Photon Factory, High Energy Accelerator Research Organization, Tsukuba, Ibaraki 305-0801, Japan

Introduction

In a previous paper [1] describing an anomalous oscillation in space (image nonprojectiveness) of equal-thickness Pendellösung fringes, we also found that equal-inclination fringes due to a minute strain center in the crystal (near the exit surface) as well show a similar anomalous oscillation. In recent experiments of Pendellösung fringes, we observed a similar equal-inclination fringe pattern showing the anomalous oscillation with a better fringe resolution than before. This observation is reported.

Experiment and results

The experiment was conducted at BL15C. The specimen was a wedge crystal of less than 2 mm in thickness, cut from a high-quality FZ silicon block. The wavelength was tuned at λ_o= 0.81 Å, the beam incident on the specimen was collimated to 0.08" in angular divergence, against 0.34" in previous experiments, and monochromated to $\Delta\lambda/\lambda_o=4\times10^{-4}$ in wavelength spread against $\Delta\lambda/\lambda_o= 9\times10^{-4}$ in previous experiments. The 220 diffraction images of the specimen were recorded by way of simultaneous imaging onto multi-stacked films.

Fig. 1 shows a set of multi-film topographs taken as described above. White contrast indicates stronger intensity here. A roughly triangular image seen in the center of each topograph is the equal-inclination fringe pattern under discussion, due to a minute strain center. From various observations, we can safely assume that the black-and-white contrast of the image is of phase contrast showing equal-inclination fringes, although strict verification is left to a future work. The background black-and-white pattern is of the main Pendellösung fringes. Nearly horizontal, faint fine striations show subsidiary fringes [2].

It is obvious that the image under discussion shows an oscillatory change among the whole multi-film topographs. It should be noted that images at front positions (near to the specimen) appear recurrently at rear positions, as T 1→T 5 (and T 6), T 2→T 8, T 4→T 7, *etc*., although the recurrence does not proceed in exactly regular way. Furthermore, steps of the continuous change of the image can be followed to some extent in the ten topographs shown. The oscillatory change with such features is quite similar to those of previous moiré and equal-thickness Pendellösung fringes. The analysis of such equal-inclination fringes would be useful for ellucidating this anomalous fringe oscillation problem.

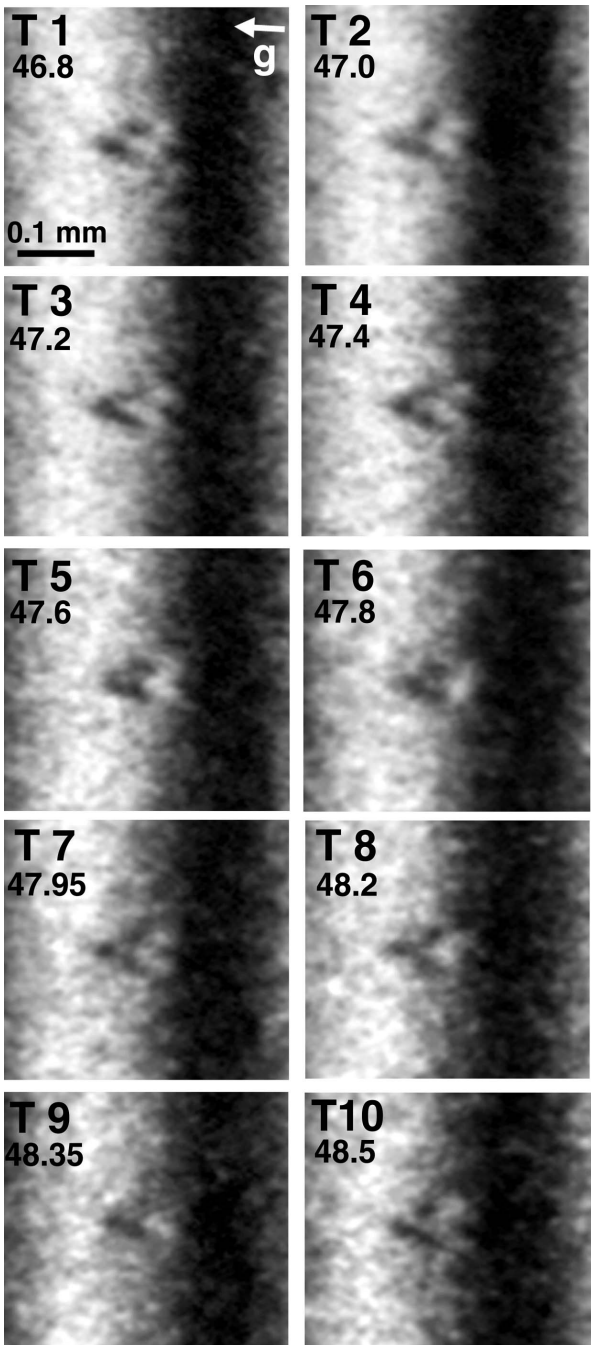

Fig. 1. Multi-film topographs showing an equal-inclination fringe pattern. Diffracted-wave image. Upper-left figures give the specimen-to-film distance in mm. Fuji #80 films (single-coated) were used. Exposure time was 25 s.

References

[1] J. Yoshimura, J. Synchrotron Rad. **7**, 374 (2000).
[2] J.Yoshimura, K.Hirano & X. Zhang, PF Activity Report #**18**, 187 (2001).

*yoshimur@ccn.yamanashi.ac.jp

15C/2000G038

Anomalous oscillation of X-ray Pendellösung fringes observed under ultra plane-wave condition (ω = 0.08”); topographic observation

Jun-ichi YOSHIMURA*[1], Keiichi HIRANO[2]
[1]Faculty of Engineering, Yamanashi University, 4-3-11 Takeda, Kofu, Yamanashi 400-8511, Japan
[2]Photon Factory, High Energy Accelerator Research Organization, Tsukuba, Ibaraki 305-0801, Japan

Introduction

We have conducted experiments of anomalous oscillation in space (image nonprojectiveness) of moiré and Pendellösung interference fringes of X-rays [1]. During the past year, the experimental research has been extended so as to use much more parallel and monochromatic beam than before. In this ultra plane-wave experiment the oscillation of Pendellösung fringes from a silicon wedge crystal was observed with a significantly improved clarity with larger amplitude than in previous experiments.

Experiment and results

The experiment was conducted at BL15C. The specimen was a wedge crystal of less than 2 mm in thickness, cut from a high-quality FZ silicon block. The wavelength was tuned at λ_o=0.81 Å. By repeating asymmetric diffraction at monochromators crystals, the beam incident on the specimen was collimated to ω=0.08” in angular divergence, against ω=0.34” in previous experiments, and monochromated to $\Delta\lambda/\lambda_o=4\times10^{-4}$ in wavelength spread, against $\Delta\lambda/\lambda_o=9\times10^{-4}$ in previous experiments. The 220 diffraction images of the specimen was recorded by way of simultaneous imaging onto multi-stacked films

Fig. 1 compares six successive member topographs of all ten multi-film simultaneous topographs in one set. White contrast indicates stronger intensity here. Equal-thickness Pendellösung fringes run vertically with a spacing of Λ=0.352 mm. Compare, for example, the topographs at heights indicated by arrows *A*, *B* and *C*. It is noted then that the distances between neighboring fringes and the local orientations of fringes oscillate among the multi-film topographs. The fringe oscillation here is produced with a much larger amplitude than in previous topographs with ω=0.34”, so that the oscillation is easily recognized by visual inspection of the topographs. In addition, anomalies in the fringe profile become more noticeable, and details of subsidiary fringe patterns [2] appear more clearly under this ultra plane-wave condition.

References

[1] J. Yoshimura, J. Synchrotron Rad. **7**, 374 (2000).
[2] J.Yoshimura, K.Hirano & X. Zhang, PF Activity Report #**18**, 187 (2001).

*yoshimur@ccn.yamanashi.ac.jp

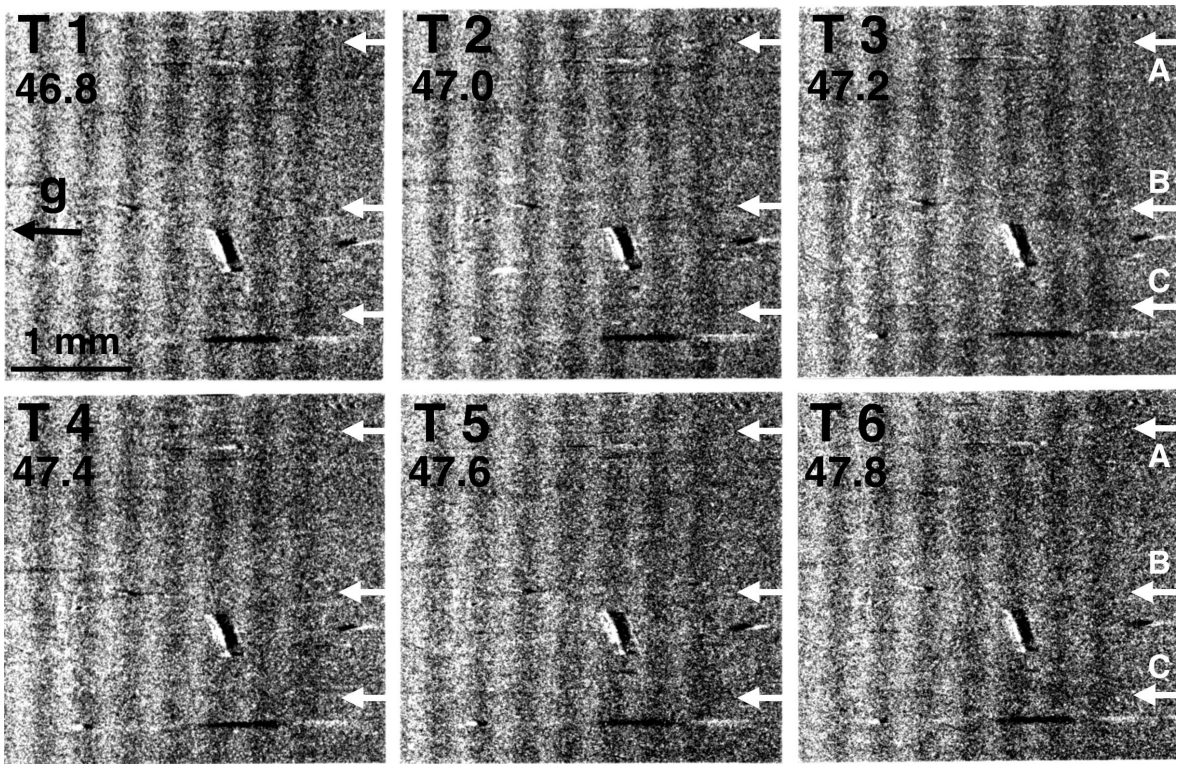

Fig. 1. Multi-film topographs showing Pendelloesung fringes. Diffracted-wave image. Taken at a deviation angle from the diffraction peak Δθ = -0.25”. Exposure time was 25 s. Upper-left figures gives the specimen-to-film distance in mm.

15C/2000G046

Study for direction of Burgers vector by resonant scattering X-ray topography

Riichirou NEGISHI[*1], Shengming ZHOU[1], Masami YOSHIZAWA[1], Tomoe FUKAMACHI[1], Isao MATSUMOTO[2] and Takaaki KAWAMURA[3]

[1]Saitama Inst. of Tech, 1690 Fusaiji, Okabe, Ohsato, Saitama 369-0293, Japan
[2]KEK-PF, 1-1 Oho,Tsukuba, Ibaraki 305-0801, Japan
[3]Yamanashi Univ. 4-4-37 Takeda, Kofu, Yamanashi 400-8510, Japan

Recently, we have taken resonant scattering topographs for a GaAs crystal with the 200 reflection using synchrotron radiation near K-absorption edges of Ga and As[1]. As shown in Fig.1, values of u and v, which are parameters describing X-ray polarizability, change from –1 to 1 with change of the incident X-ray energy. The variations of contrasts in lattice defect images, reflecting characteristics of (u, v) = (1,0), (-1,0), (0,-1) and (0,1), were reported in reference [1]. In this report, we present results of the correlation between the sign change of v and Burgers vector ***b***. The optical system for the experiment is the same as that in [1]. Fig.2 shows topographs recorded for 020 and 220 reflections at the energy indicated by A in Fig.1, respectively. The darker region corresponds to the stronger intensity. Consequently, ***b*** is located in a plane perpendicular to $\boldsymbol{h}_{110}$, and this can be confirmed by the disappearance of an image indicated by a white arrow in Fig.2 (b).

The calculated rocking curves, corresponding to points B with (u, v) = (0,-1) and D with (0, 1) in Fig.1, are shown in Fig.3 (a) and (b). The transmitted rocking curve (P_d) is asymmetric with respect to the exact Bragg angle, although the diffracted one (P_h) is symmetric, and the both exhibit Borrmann effect conspicuously. There is a tail at higher angle side of the transmitted rocking curve in (a), but at lower angle side in (b).

The transmitted-beam images recorded at the conditions corresponding to the points of B and D are shown in Figs.4 (a) and (b). The images of the lattice defects turn into double white lines, because that Borrmann effect is disturbed by the shift of Bragg angle in the region with distorted lattices. It is noted that the image contrasts of the double line in the region enclosed by , the left side is brighter than the right side in (a), but the right side is brighter in (b). Although the contrast difference is much smaller in than that in , it still can be seen in that the left-upper side of the double lines is brighter in (a), and the right-lower side is brighter in (b). The lattice defect images comprising of double lines suggest that the defects belong to an edge dislocation. According to the changes in the contrasts of the left-upper and right-lower of the double line inside , it can be concluded that the direction of ***b*** is $[\bar{1}10]$, parallel to the crystal surface (paper surface) as indicated by the black-bold arrow. Here, ***b*** is defined by FS/RH (Finish Start/Right-Hand). On the other hand, as to the defect regions enclosed in , reflection surface at the left part in the double lines bends this side with respect to the reflection surface for the exact Bragg angle, but that at the right part bends the opposite side, and then the direction of ***b*** is estimated to be $[\bar{1}01]$. According to the aforementioned discussion, it is clear that direction of Burgers vector ***b*** can be determined by using contrast changes caused by sign change of v known as an effect of resonant scattering dynamical diffraction.

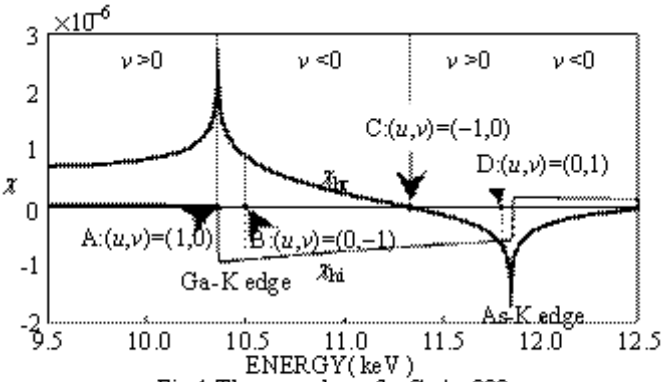

Fig.1 The χ_{hr} and χ_{hi} for GaAs 200.

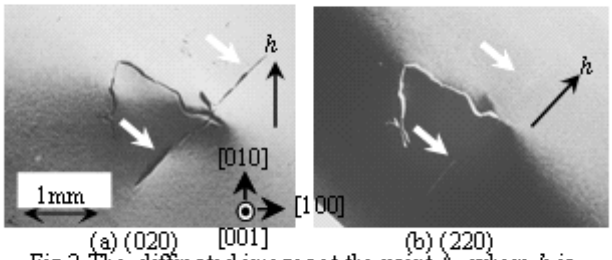

Fig.2 The diffracted images at the point A, where h is reciprocal lattice vector.

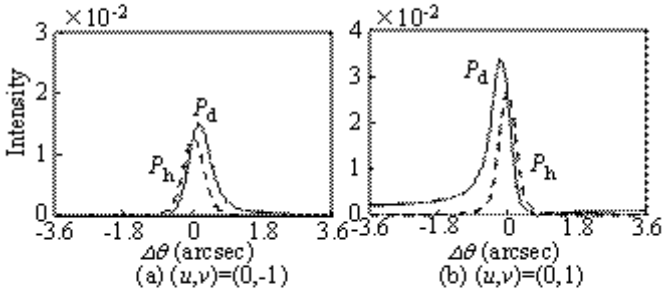

Fig.3 The calculated rocking curves of GaAs200 with crystal thickness 121 μm.

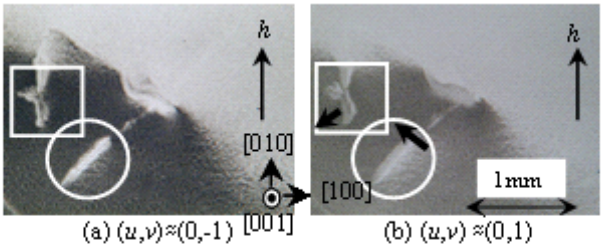

Fig.4 The transmitted-images.

References
[1] R. Negishi et al., Jpn. J. Appl. Phys. 40, L884 (2001).
*negishi@sit.ac.jp

15C/2000G046

Determination of anomalous scattering factor near Ge-K absorption edge used by phase change method

Masami YOSHIZAWA*[1], ShengMing ZHOU[1], Riichirou NEGISHI[1], Isao MATSUMOTO[2], Tomoe FUKAMACHI[1] and Takaaki KAWAMURA[3]
[1]Saitama Institute of Tech., Fusaiji, Okabe, Saitama 369-0293, Japan
[2]KEK-PF, Tsukuba, Ibaraki 305-0801, Japan
[3]Yamanashi Univ., Kofu, Yamanashi 400-8510, Japan

The anomalous scattering factor ($f'+if''$) (ASF) of X-ray resonant scattering changes remarkably near an absorption edge of an atom. It is well known that this change is significant for the phase determination of crystal structure factor and the study of X-ray magnetic scattering. ASF near the absorption edge is so sensitive to the conduction band structure and the lifetime of intermediate transition process that it is not easy to evaluate it theoretically. Thus, it is interesting to investigate the consistency between the calculated ASF and the measured one. When the sign of Fourier coefficient χ_{hr} (χ_{hi}) of real (imaginary) part of X-ray polarizabilty changes, a conspicuous change of asymmetry in rocking curves (Fig.1) can be seen in a perfect crystal. We have studied the phase changes of χ_{hr} (or f^0+f', f^0 is the normal atomic scattering factor) using rocking curves for 660, 555 and 844 reflections of Ge at BL-15C in KEK-PF. At the boundary of the phase change, the condition of $f^0+f'=0$ can be found experimentally. Then the value of f' can be determined with good precision using the well-known calculated value of f^0.

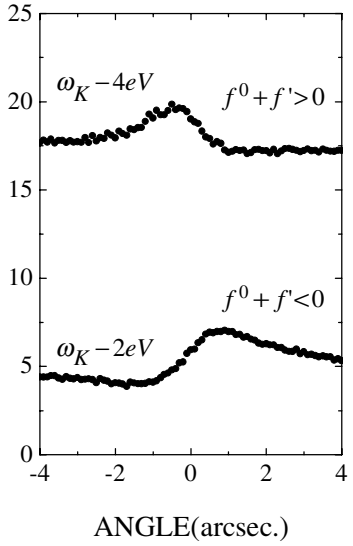

Fig.1 Observed rocking curves of Transmitted-beam for Ge 844. ω_K is the energy of Ge K-absorption edge (11103.6eV).

The calculated and measured ASFs are shown in Fig.2. The thin solid line (corrected by lifetime) and the dotted one (without correction) are obtained according to the isolated atom model (IAM). The thick solid line and the open circles are obtained as follows. f' for the former is determined by the dispersion relation (DR)[1)] and for the latter by the phase change method (PCM), whereas f'' is determined from the measured XAFS in both cases. It is clear that the value of f' determined by the PCM is different from that calculated by the IAM , but is in excellent agreement with that obtained by the DR.

References

1) T. Kawamura and T. Fukamachi: Jpn. J. Appl. Phys. **17** (1978) Sppli. 17-2,224-226.
2) L. G. Parratt and C. F. Hempstead: Phys. Rev. **94** (1954) 1593-1600.
3) S. Sasaki: KEK Report 88-14 M/D, (1989) 1-136.

* yoshizaw@sit.ac.jp

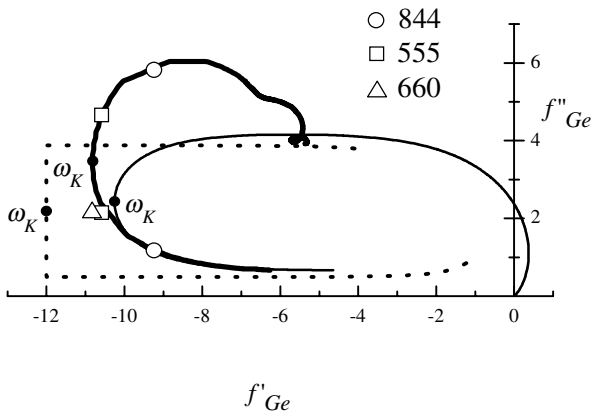

Fig.2 The calculated and measured ASF. The thin solid line is calculated by Parratt and Hempstead formula[2)]. The dotted line is calculated by Sasaki[3)].

6A/2001C018

Impurity effects on protein crystal quality

Izumi YOSHIZAKI[1*], Noriyuki IGARASHI[2], Hirohiko NAKAMURA[1],
Yoshikazu IIMURA[3], Seijiro FUKUYAMA[3]
[1] Space Utilization Research Center, National Space Development agency of Japan,
2-1 Sengen, Tsukuba, Ibaraki, 305-8505 Japan
[2] KEK-PF, 1-1 Oho, Tsukuba, Ibaraki 305-0801, Japan
[3] Advanced Engineering Service, Co. Ltd., 1-6-1 Takezono, Tsukuba, Ibaraki, 305-0032 Japan

Introduction

There have been many attempts of protein crystal growth experiments in microgravity, and thousands of samples have been analysed [1]. It has been reported that microgravity had a positive effect on the crystal quality in many of the samples [2,3]. The effect of microgravity is generally understood as follows: (1) Because of the absence of convection, the depleted zone, i.e. a zone where the protein concentration is lower than the bulk solution because of protein consumption by the growing crystal, around the growing crystal will be maintained and growth will proceed slowly [4,5], (2) Because of the absence of convection, impurities which are preferentially incorporated into the crystal surface will initially be incorporated into the crystal, but later an impurity depletion zone will form which results in less impurity incorporation into the crystal [5,6], (3) Because of the absence of sedimentation, microcrystals formed in the bulk solution do not deposit on the growing crystal [4,7].

We have already proved that the crystal quality actually increases when the supersaturation is lower by using PF BL6A [8]. This supports the above-mentioned first possibility of microgravity effect. In this study, we focus on the above-mentioned second possibility that the impurity deteriorates the crystal quality. If impurity incorporation decreases the crystal quality, microgravity may work as a positive impurity filter.

Experiment

Materials and methods

Hen Egg White Lysozyme tetragonal crystals for X-ray data collection were crystallized by the conventional batch method at a temperature of 20 ºC. Lysozyme dimer was used as a model impurity. Covalently bound lysozyme dimer was purified from commercial lysozyme sample by re-crystallization, gel filtration and HPLC. 93% pure dimer sample was added to 99.99% pure lysozyme monomer sample for crystallization in various rates; 0%, 0.5%, 2% and 5%.

The crystal size was carefully controlled to be the same to compare the crystal quality without compensation. We collected all data at room temperature at the BL-6A of the Photon Factory (PF), Tsukuba, Japan. Nearly complete diffraction data sets were collected using an ADSC Quantum 4R CCD detector by the oscillation method with a wavelength of 0.978 Å. Fifteen samples were analyzed in total. The X-ray diffraction data were auto-indexed and integrated using the program *DPS/MOSFLM/CCP4* [9] and then merged and scaled with *SCALA/CCP4* [10].

Results

The crystal quality was evaluated by four indexes; maximum resolution limit, $\langle I \rangle / \langle \underline{\sigma} I \rangle$, R_{merge}, overall B factor. In every index, there was a tendency that the crystal quality decreased as the impurity improved. The results will be reported in detail elsewhere.

NASDA is planning a microgravity experiment on a space shuttle on 2002. The impurity incorporation in space and the crystal quality of space grown crystals will be studied.

References

[1]http://mgravity.itsc.uah.edu/microgravity/micrex/micrex.stm
[2] L.J. DeLucas *et al.*, Science **246** (1989) 651-654.
[3]http://www.reston.com/nasa/ascb/07.20.98.delucas.html
[4] A. McPherson, J. Phys. **D 26** (1993) B104-B112.
[5] A. McPherson *et al.*, J. Crystal Growth **196** (1999) 572-586.
[6] A.A. Chernov, J. Crystal Growth **174** (1997) 354-361.
[7] A. McPherson, In *Crystallization of Biological Macromolecules*: Cold Spring Harbor Laboratory Press (1999) 453-455.
[8] I. Yoshizaki *et al.*, Acta Cryst. **D57** (2001) 1621-1629.
[9] M. G. Rossman, C. G. van Beek, Acta Cryst. **D55** (1999) 1631-1640
[10] Collaborative Computational Project (1994), Number 4, Acta Cryst. **D50**, 760-763

* yoshizaki.izumi@nasda.go.jp

18B/2001G164

Crystal structure of 23S rRNA-binding protein L13 from hyperthermophilic archaeon *Pyrococcus horikoshii*

Takashi NAKASHIMA, Mai TANAKA, Min YAO*, Nobuhisa WATANABE, Isao TANAKA

Hokkaido Univ., N8W10, Kita-ku, Sapporo 060-0810, Japan

Introduction

Ribosome, the enormous complex of proteins and RNAs, plays a principal role in the biosynthesis of protein. Recently, studies of the entire structure of ribosome, and the complex structure of ribosomal protein and rRNA have been rapidly advanced. Much information about translational mechanism was obtained from these results. The ribosomal assembly runs through a series of intermediate particles with increasing S-values, (i.e. increasing compactness). Ribosomal protein L13 is one of early assembly proteins essential for the functionally important conformational state during the early assembly. Ribosomal protein L13 is one of primary 23S rRNA-binding proteins. Three-dimensional structure of L13 may give structural basis on the principles of protein-RNA recognition.

Table 1. Data collection and refinement statistics

Wavelength (Å)	1.0
Temperature	room temperature
Space group	$P2_12_12_1$
Cell parameters (Å)	a = 41.08
	b = 51.54
	c = 64.20
Resolution (Å)	22.7-1.6 (1.69-1.60)
Total reflections	124,718
Unique reflections	17,561
Completeness (%)	94.8 (77.2)
Redundancy	7.1 (6.6)
R_{meas} (%)	3.3 (14.8)
Averaged $I/\sigma(I)$	12.6 (5.0)
Resolution range (Å)	8.0-1.6
Number of reflections	17,382
Residues included	127
Number of non-hydrogen atoms	
protein	1,038
solvent	300
R-factor (%)	21.2
R_{free} –factor (%)	22.7
Average B factor (Å^2)	24.42
Rms deviations	
bond lengths (Å)	0.0044
bond angles (°)	1. 15
dihedral angles (°)	21.5

Values in parentheses are for the outermost resolution shell.

Results

Ribosomal protein L13 from hyperthermophilic archaeon *Pyrococcus horikoshii* (PhoL13) was crystallized at 20°C by the hanging-drop vapor diffusion technique. The crystal of native PhoL13 was mounted a glass capillary. X-ray diffraction data set for native PhoL13 was collected up to 1.6 Å resolution at room temperature using the ADSC CCD detector and synchrotron radiation with 1.0 Å wavelength. Data were processed with MOSFLM and scaled with SCALA. Crystal of *Pho*L13 belongs to the space group $P2_12_12_1$, with unit-cell parameters of a=41.08 Å, b=51.54 Å and c=64.20 Å. The cell parameters of native PhoL13 were slightly different from ones of Se-Met PhoL13.

The structure of *Pho*L13 was determined by MAD method using Se-Met MAD data set, which was collected up to 1.8 Å resolution using cryogenic technique previously. Because the native crystal was not isomorphous with the Se-Met L13 crystal, a native PhoL13 model (Fig. 1) was obtained by molecular replacement using program AMORE. The model was rebuild on the electron density map after positional and temperature factor refinements. These steps were repeated several cycles and water molecules were added. The data collection and refinement statistics are summarized in Table 1. The structure detail of PhoL13 will be published elsewhere.

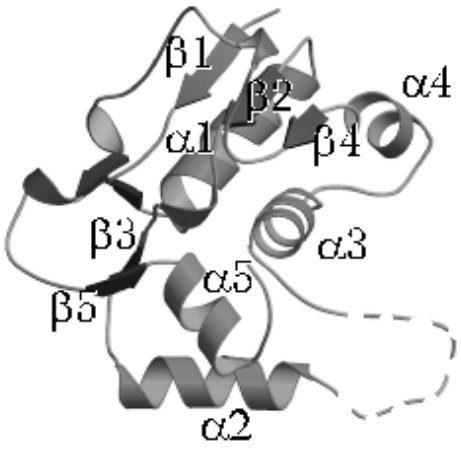

Figure 1. Ribbon diagram of *Pho*L13. The disordered region (residue 53-67) was connected with a dashed line.

References

[1] T. Nakashima et al., in preparation for publication.

* yao@castor.sci.hokudai.ac.jp

4B2/2001G188

Crystal structure determination of $(H_2pc)_3 PF_{6-x}Cl_x$ by synchrotron powder diffractometry

Takashi IDA*[1], Fumiharu SATO[1], Hiroyuki OKUNO[2], Hideo YAMAKADO[2] and Hideo TORAYA[1]
[1]CRL, Nagoya Inst. Tech., Tajimi, Gifu 507-0071, Japan
[2]Wakayama Univ., Wakayama 640-8510, Japan

A new partially oxidized metal-free phthalocyanine (H_2pc) salt was electrochemically synthesized from neutral H_2pc in 1-chloronaphthalene solution with $(n\text{-}Bu)_4N\ PF_6$ as the electrolyte. The electric conductivity along the growth axis of a needle-like crystal was about 9 S cm^{-1} at room temperature. The results of chemical analysis have implied that the composition is nominally $H_2pc\ (PF_{5.28}Cl_{0.72})_{0.28}$. It has been suggested that the fluorine atoms in the PF_6 ions were partly substituted by chlorine atoms during the electrochemical process.

Powder X-ray diffraction data have been collected with a high-resolution powder diffractometer MDS [1] on beamline BL4B2 at the Phothon Factory. The incident beam wavelength was 1.2072(4) Å. A Lindemann glass capillary of 1.0 mm ϕ in diameter filled with 9 mg of the grinded powder sample was used as the specimen for the powder diffraction measurement. The collected diffraction data range was 1 to 150º in 2θ at a step size of 0.004º using a counting time of 8 s per point.

All the detectable diffraction peaks were indexed by assuming a rhombohedral (*R*3) unit cell with the refined lattice parameters of a = 21.3427(4) Å and α = 119.42784(2)º. The cell volume of 1909.5(1) $Å^3$ indicates the existence of three H_2pc molecules in the unit cell. The periodicity of 4.8687(2) Å along the [111] direction coincides with the observed periodicity along the growth axis in the oscillation photograph taken for a bundle of thin needle-like crystals in our laboratory.

The chemical composition of $(H_2pc)_3\ PF_{6-x}\ Cl_x$ was assumed to satisfy the requirement of the symmetry. The powder diffraction pattern was simulated for further simplified composition, $(H_2pc)_3\ PF_6$ (x = 0). The position and orientation of the H_2pc and PF_6 molecules were optimized by a least-squares method to fit the observed diffraction intensity data, treating H_2pc and PF_6 molecules as rigid bodies. The common isotropic atomic displacement parameter of 0.01 $Å^2$ was assumed for all the atoms.

Figure 1 shows the experimental powder diffraction data, calculated curve for the optimized structure of $(H_2pc)_3 PF_6$, and the difference plot. The reliability factor for the profile fitting was 11.89 %.

The projection of the refined crystal structure along the [111] direction is shown in Fig. 2. H_2pc molecules are uniformly stacked along the [111] direction. The optimized angle between the [111] and the normal direction of the H_2pc molecular plane was 46.88(1)º, which gives the interplanar distance between the neighboring H_2pc molecules to be 3.33 Å. The orientation of each H_2pc molecule relative to the stacking axis is very similar to that of the X-polymorph of neutral H_2pc [2].

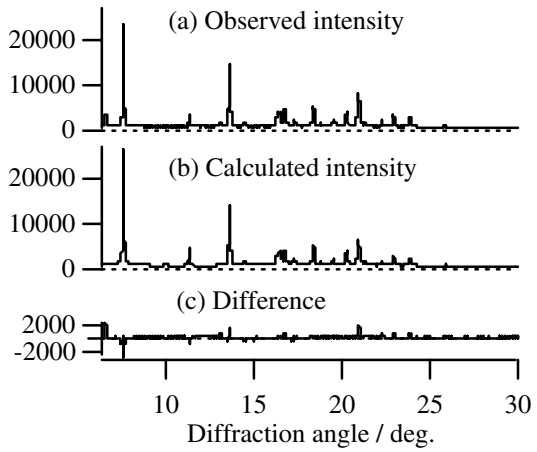

Fig. 1 (a) Synchrotron powder diffraction pattern of $(H_2pc)_3\ PF_{6-x}\ Cl_x$, (b) calculated curve for the optimized $(H_2pc)_3\ PF_6$, and (c) the difference.

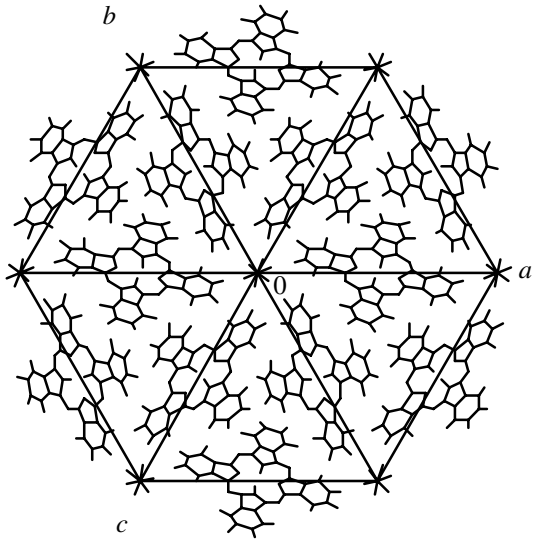

Fig. 2 Projection of the optimized crystal structure of $(H_2pc)_3\ PF_6$.

References

[1] H. Toraya et al., J. Synchrotron Rad. 3, 75 (1996).
[2] R. B. Hammond et al., J. Chem. Soc. Perkin Trans. 2, 1527 (1996).

* ida@crl.nitech.ac.jp

3A/2001G241

Synchrotron X-ray diffraction analysis of pulse-heated Orgueil carbonaceous chondrite : experimental reproduction of micrometeorites

Wataru NOZAKI*[1], Tomoki NAKAMURA[1], Takaaki NOGUCHI[2]
[1]Earth Planet. Sci., Kyushu University, Hakozaki, Fukuoka 812-8581, Japan.
[2]Materials and Biological Sci., Ibaraki University, Bunkyo, Mito 310-8512, Japan

Introduction

Micrometeorites are small (<1mm) extraterrestrial material, which constitute the major fraction of extraterrestrial material fall onto the Earth [1,2]. To identify their parent body is one of the major objective of micrometeorite researches. Although bulk mineralogy provides an important clue to the origins of micrometeorites, primary mineralogy of micrometeorites has been altered by various degrees of heating during atmospheric entry. Thus, it is important to clarify the mineralogical changes in micrometeorites during atmospheric entry heating.

Experiment

We performed pulse-heating experiments of a small piece of Orgueil (CI1) carbonaceous chondrite from 200ºC to 1000ºC with 100°C interval under ambient atmospheric pressure of 1.5x10-2 torr. In each step, the sample was heated for 120 sec and bulk mineralogy was analyzed by X-ray diffraction with monochromatic X-rays of 2.164 Å wavelength at the beamline 3A.

Results

Before heating, the Orgueil sample consisted of saponite, serpentine, magnetite, ferrihydrite, carbonate (dolomite), Ca-sulfate, and minor amount of Fe-Sulfide. By heating at 200 and 300ºC, the bulk mineralogy did not change. At 400ºC, diffraction peaks of Ca-sulfate disappeared and those of newly formed anhydrite appeared. Relative intensity of diffraction peaks of serpentine decreased at 500ºC and disappeared at 600ºC. Intensities of diffraction peaks of saponite decreased and the basal spacing (001) of saponite shrunk to ~12Å at 600ºC. Diffraction peaks of saponite were hardly identified at 700ºC. TEM observation of another Orgueil sample heated at this temperature revealed both of saponite and serpentine have only remnant layer structure and the majority of them are almost completely decomposed into amorphous material. Dolomite and ferrihydrite also decomposed at 700ºC. At 800ºC, newly formed olivine and Fe-oxide (magnesiowüstite) appeared. At 900 to 1000ºC, the abundance and crystallinity of olivine increased progressively.

Discussion

Phyllosilicate-bearing micrometeorites are thought to be the least heated samples, because saponite and serpentine are decomposed below ~700ºC [3]. Most of phyllosilicate-bearing micrometeorites can be classified into three major mineralogical types based on the major minerals in them; type A: mainly consist of saponite, serpentine, and magnetite, type B: saponite and magnetite, and type C: serpentine [4]. We also found micrometeorites that consist of amorphous material and magnetite (hereafter type D).

It is likely that type A and B micrometeorites were formed by weak heating of CI chondrite-like material, which is composed mainly of saponite, serpentine, and magnetite. Because serpentine is decomposed at lower temperature than saponite, it is plausible that serpentine was preferentially decomposed into amorphous material by weak atmospheric entry heating. Therefore, there is a possibility that type B micrometeorites were made from CI chondrite-like material.

The heating experiments show that the mineralogy of the Orgueil sample heated below 500ºC matches well with that of type A phyllosilicate-rich micrometeorites. The Orgueil sample heated at 600ºC, where serpentine has decomposed while saponite and magnetite still remains, show similar bulk mineralogy to type B micrometeorites. However, there is a great difference in mineralogy between the heated Orgueil sample and type B micrometeorites. In the heated Orgueil sample, basal spacing of saponite has shrunk down to ~12Å by weak heating, while that in the majority of the type B micrometeorites show no shrinkage (13 ~ 14Å), suggesting that type B micrometeorites have not been heated above 600ºC and originally not contained serpentine. Thus, precursor material of type B micrometeorites may contain abundant saponite and magnetite, such mineralogy can be found in 'Carbonate-poor lithology' of Tagish Lake CI2 chondrite [5,6].

References

[1] E. Grün et al., Icarus 62, 244 (1985).
[2] S. G. Love and D. E. Brownlee, Science 262, 550 (1993).
[3] W. Nozaki et al., MAPS, 36, A151 (2001).
[4] T. Noguchi et al., NIPR, 27, 130 (2002).
[5] M. Gounelle et al., LPSC 32I, #1616 CD-ROM (2001).
[6] T. Mikouchi et al., LPSC 32, #1371 CD-ROM (2001).

* wataru@geo.kyushu-u.ac.jp

10B/2001G320

Local structure of Zr incorporated in ETS-10 titanosilicate

Yasuhide GOA[1], Hideaki YOSHITAKE[2], Peng WU[3], Takashi TATSUMI[*3]
[1]Graduate School of Engineering, The University of Tokyo, Hongo, Bunkyo-ku, Tokyo, 113-8656, Japan
[2]Graduate School of Environment and Information Sciences, Yokohama National University, Tokiwadai, Hodogaya-ku, Yokohama 240-8501, Japan
[3]Graduate School of Engineering, Yokohama National University, Tokiwadai, Hodogaya-ku, Yokohama 240-8501, Japan

Introduction

ETS-10 is one of crystalline microporous titanosilicates with corner-sharing SiO_4 tetrahedra and TiO_6 octahedra linked through bridging oxygen atoms [1], which leads us to a great interest in the ion-exchange or adsorption characteristics of the material. Here we studied on the substitution of framework sites with Zr and the local structure of Zr in ETS-10 structure.

Experimental

ETZrS-10 was hydrothermally synthesized from the gel with a chemical composition of 5 SiO_2 · TiO_2 · 0.3 ZrO_2 · 3 NaOH · KF · 75 H_2O at 473 K for 45 h, using Ludox® TM-40 colloidal silica and P25 titania powder as Si and Ti source, respectively. XRD was performed to confirm the crystallinity of the material. Zr K-edge spectra were collected at BL-10B in a transmission mode and the data were analyzed by REX 2000 (Rigaku).

Results and discussion

XRD patterns proved that the obtained products contained mainly ETS-10 phase and only small amount of anatase TiO_2 by-phase. Elemental analysis indicated that Zr/Ti ratio in the product was 0.30, comparable to that in the mother gel.

Fig.1 shows the Fourier transforms of the k^3-weighed EXAFS oscillation of ETZrS-10 material. The curve-fitting results are summarized in Table 1. The obtained coordination numbers of Zr-Ti and Zr-Si are consistent with that one Zr atom links with two OTi and four OSi, namely in a (4Si, 2Ti) coordination environment. We examined whether other structural models, such as $Zr(OSi)_4$ (4Si) and $Zr(OSi)_3(OTi)_1$ (3Si, 1Ti), substituting tetrahedral Si, and $Zr(OZr)_6$ (bulk zirconia), would fit our EXAFS results; however none of them led to good fitting results. This strongly indicates that Zr atom substituted framework octahedral Ti isomorphously, being isolated. Interestingly, our findings are quite different from the observations by Eldewik et al. on the substitution with cobalt [2]. According to their results, Co substituted tetrahedral Si at (3Si, 1Ti) site. This difference of the site might be caused by the larger ionic radius of Zr^{4+} than that of Co^{2+}.

Table 1 Results of curve fitting analysis

Scattering atom	N	R / Å	dE / eV	DW / Å	R / %
O	4.429	2.092	-1.122	0.055	5.7
Ti	1.509	3.801	-12.322	0.068	
Si	3.458	3.481	9.345	0.060	

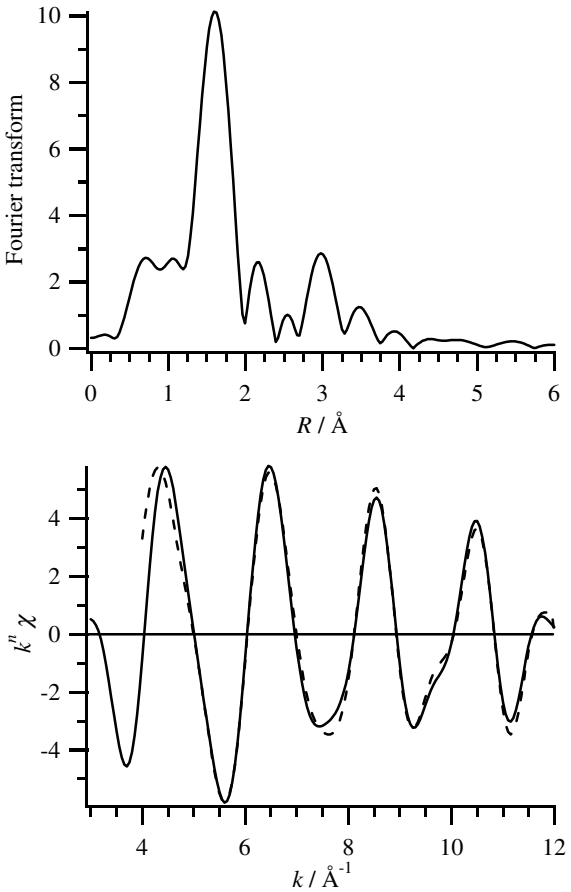

Fig.1 Fourier transform (a) and the fit to back Fourier transforms (b) of ETZrS-10. Solid line: experimental data, dashed line: simulated data.

References

[1] M.W.Anderson et al., *Nature*, **367**, 347 (1994)
[2] A. Eldewik et al., *Microporous Mesoporous Mater.*, **48**, 65 (2001)

* ttatsumi@ynu.ac.jp

4B2/2001P003

Quantitative analyses of Brazil twin defects in chalcedony by X-ray powder diffraction method

Toshiro NAGASE[1*], Masahiro ABIKO[2], Masahiko TANAKA[3]
[1]The Tohoku University Museum, Sendai 980-8578, Japan
[2] Institute of Mineralogy, Petrology, and Economic Geology, Faculty of Science, Tohoku University, Sendai 980-8578, Japan
[3]KEK-PF, Tsukuba, Ibaraki 305-0801, Japan

Introduction

Chalcedony and agate have been recognized as aggregates of submicron-sized quartz crystals. However, recent transmission electron microscopy (TEM) observations[1] reveal that chalcedony commonly includes new silica polymorph, "moganite", which structure is similar to that of modified quartz by Brazil twinning[2-3]. The quartz crystal precipitated from low-temperature solution is known to be characterized by intergrowth with moganite and/or development of Brazil twin lamellae.

In this study, XRD measurements on synthetic submicron-sized quartz crystals and natural chalcedony samples were carried out to clarify the growth process of moganite and genesis of Brazil twin lamellae.

Experimental

Experimental samples are listed in Table 1. The synthetic samples were obtained by re-crystallization from silica gel (Wako Q-22) in 0.1N KOH solution at 175-225°C. Natural chalcedony (agate) samples were collected from Brazil, and Hosaka, Fukushima Prefecture, Japan. SR resonant powder diffraction data collections were carried out with multiple-detector system (MDS) installed at the BL-4B2 station. The step scan widths were 0.004° or 0.005° in 2θ and fixed counting times were 1.5 or 2 sec. The wave length of the incident X-ray was 1.2 Å.

Table 1. List of measured samples

Sample No.	Occurrences	Growth temp. (°C)	Mature times (hours)
1	Natural chalcedony (Hosaka, Fukushima)	-	-
2	Natural chalcedony (Hosaka, Fukushima)	-	-
3	Natural agate (Brazil)	-	-
4	Synthetic	175	363
5	Synthetic	175	576
6	Synthetic	200	171
7	Synthetic	200	250
8	Synthetic	225	100

Results and Discussion

The results of cell parameter refinement of quartz crystals in the samples are shown in Figure 1. The unit cell dimensions show slightly different trends between the synthetic and the natural samples. In the synthetic samples, the unit cell dimensions are reduced with increasing temperature and mature time of growth. Peak fitting analyses also shows different crystallographic directions of strain in the synthetic and natural crystals.

Our TEM observations show that the synthetic samples are composed of quartz and moganite that includes numerous planar defects. However, a characteristic reflection of moganite could not be detected in the synthetic samples by the XRD analyses using SR. This result suggested that an amount of moganite crystal is too little in the synthetic sample to be detected and/or that the highly disordered structure with planar defects reduce intensity of the reflection. Although moganite nucleates only at the initial stage of the crystallization of quartz crystals, moganite do not grow at the following growth stage. A kinetic process causes the moganite crystal at the nucleation stage of the silica precipitation.

The authors thank to Prof. H. Toraya (Nagoya Inst. Tech.) for kindly help in data collection at PF.

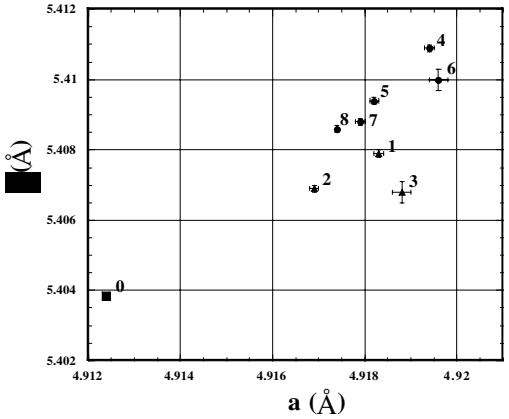

Figure 1. Variation of unit cell dimensions of measured samples. The number in the figure corresponds to the sample number in Table 1. No. 0: the bulk quartz crystal measured by Will et al.[4]

References

[1] H. Xu et al., *Amer. Mineral.*, **83**, 542, (1998).
[2] G. Miehe et al., *Z. Kristallogr.*, **182**, 183 (1988).
[3] G. Miehe and H. Graetsch, *Eur., J. Mineral.*, **4**, 693 (1992).
[4] G.Will et al., *J. Appl. Cryst.* **21**, 182, (1988).
* nagase@mail.cc.tohoku.ac.jp